Research Square

Preprints are preliminary reports that have not undergone peer review.
They should not be considered conclusive, used to inform clinical practice,
or referenced by the media as validated information.

4-Methylumbelliferone induces oxidative stress-driven metabolic vulnerability and disrupts glycosylation in glioblastoma cells

Daniela Poodts
Universidad de Buenos Aires, Facultad de Farmacia y Bioquímica; Departamento de Microbiología, Inmunología y Biotecnología; Instituto de Estudios de la Inmunidad Humoral (IDEHU)- CONICET

Leonardo Pellizza
Instituto de Investigaciones Bioquímicas de Buenos Aires (IIBBA-CONICET)- Fundación Instituto Leloir

Martín Manuel Ledesma
Unidad de Conocimiento Traslacional, Hospital de Alta Complejidad del Bicentenario de Esteban Echeverría, CIBiMet-CONICET

Magalí Gretel Ferreira
Centro de Oncología Molecular, Universidad Nacional de Quilmes

Facundo Nuñez
Universidad de Buenos Aires, Facultad de Farmacia y Bioquímica; Departamento de Microbiología, Inmunología y Biotecnología; Instituto de Estudios de la Inmunidad Humoral (IDEHU)- CONICET

Candela Miraglia
Universidad de Buenos Aires, Facultad de Farmacia y Bioquímica; Departamento de Microbiología, Inmunología y Biotecnología; Instituto de Estudios de la Inmunidad Humoral (IDEHU)- CONICET

Paloma Gueller
Universidad de Buenos Aires, Facultad de Farmacia y Bioquímica; Departamento de Microbiología, Inmunología y Biotecnología; Instituto de Estudios de la Inmunidad Humoral (IDEHU)- CONICET

Nicolás Seveso
Universidad de Buenos Aires, Facultad de Farmacia y Bioquímica; Departamento de Microbiología, Inmunología y Biotecnología; Instituto de Estudios de la Inmunidad Humoral (IDEHU)- CONICET

Silvia Elvira Hajos
Universidad de Buenos Aires, Facultad de Farmacia y Bioquímica; Departamento de Microbiología, Inmunología y Biotecnología; Instituto de Estudios de la Inmunidad Humoral (IDEHU)- CONICET

Mariano Gabri
Centro de Oncología Molecular, Universidad Nacional de Quilmes

Martín Arán
Instituto de Investigaciones Bioquímicas de Buenos Aires (IIBBA-CONICET)- Fundación Instituto Leloir

Silvina Laura Lompardía

Universidad de Buenos Aires, Facultad de Farmacia y Bioquímica; Departamento de Microbiología, Inmunología y Biotecnología; Instituto de Estudios de la Inmunidad Humoral (IDEHU)- CONICET

Matías Arturo Pibuel

pibuelmatias@gmail.com

Universidad de Buenos Aires, Facultad de Farmacia y Bioquímica; Departamento de Microbiología, Inmunología y Biotecnología; Instituto de Estudios de la Inmunidad Humoral (IDEHU)- CONICET

Article

Keywords: Glioblastoma, 4-methylumbellifeorne, NAD, metabolomic, glycosylation

Posted Date: July 7th, 2026

DOI: https://doi.org/10.21203/rs.3.rs-10083589/v1

License: This work is licensed under a Creative Commons Attribution 4.0 International License. Read Full License

Additional Declarations: No competing interests reported.

Version of Record: A version of this preprint was published at Scientific Reports on October 5th, 2026. See the published version at https://doi.org/10.1038/s41598-026-73033-5.

Abstract

Background: Glioblastoma (GBM) is an aggressive brain tumor characterized by high metabolic plasticity and resistance to standard therapies. Targeting metabolic vulnerabilities has emerged as a promising therapeutic strategy. 4-Methylumbelliferone (4MU), a known inhibitor of hyaluronan synthesis, has demonstrated antitumor effects beyond its canonical mechanism; however, its impact on tumor metabolism and associated pathways in GBM remains poorly understood.

Methods: Human glioblastoma cell lines (U251 and LN229) were treated with 4MU (1000 μM) or vehicle. Metabolic alterations were assessed using untargeted ^{1}H-NMR-based metabolomics, followed by metabolite set quantitative enrichment analysis (QEA). Oxidative stress was evaluated using a dihydrorhodamine (DHR) assay. N-glycosylation patterns were analyzed by lectin-binding assays and flow cytometry. Glycolytic activity was determined using a Seahorse Glycolysis Stress Test. Statistical analyses included Student's t-test, one-way ANOVA, and multiple comparison tests, considering $p < 0.05$ as significant.

Results: 4MU rapidly induced oxidative stress in both glioblastoma cell lines, detectable as early as 1.5 hours. This early redox imbalance preceded broader metabolic alterations observed at 24 hours, including significant depletion of NAD^+ levels and an increase in $NADP^+$. Metabolomic and enrichment analyses revealed disruption of central metabolic pathways, particularly those related to nucleotide sugars and glycosylation. Consistently, lectin-binding assays confirmed altered N-glycosylation patterns in both cell lines. Additionally, 4MU treatment increased glycolytic activity in U251 cells, suggesting a compensatory response to redox and bioenergetic stress.

Conclusions: These findings support a model in which 4MU induces an early oxidative stress-driven metabolic vulnerability in glioblastoma cells, leading to NAD^+ depletion, metabolic rewiring, and impaired glycosylation. This integrated response may contribute to the cytostatic effects previously described for 4MU and highlights metabolic pathways that could be therapeutically exploited. Our results provide new mechanistic insights into the antitumor activity of 4MU and support its potential repositioning as a strategy targeting metabolic vulnerabilities in GBM.

BACKGROUND

Glioblastoma (GBM) is the most malignant primary brain tumor. Although recent advances in cancer therapy improved the outcome of several tumors, for the past two decades there were no significant changes in GBM(1,2). Under the current protocol of treatment, based on surgical resection, radio, and chemotherapy, patients with GBM have a median survival time of 14.5 months(3). The first-line drug used on these patients is temozolomide, which has several adverse effects. Not only that, but also nearly 50% of patients are or become refractory to this drug(2,4). This situation exposes the need to search for and develop new therapeutic alternatives.

In this way, several groups described possible compounds as chemotherapy adjuvants. In our case, we have demonstrated the promising effect of 4-methylumbelliferone (4MU) on both murine and human GBM cells(5–7). Moreover, we showed that this drug has no toxic effect on normal brain models and even verified that this drug acts selectively on GBM cells without affecting normal brain cells when both models are co-cultured(7). Remarkably, 4MU is approved in Asia and Europe as a choleretic and antispasmodic agent and recently it was repurposed to be used in liver fibrosis(8–11). Therefore, its use as an anticancer drug would represent a drug reposition with all the advantages of the case.

4MU is a coumarin derivative without adverse effects reported, even under long-term administration protocols(8,10). This drug was first used as a hyaluronan synthesis inhibitor since it depletes the cell of UDP-glucuronic acid, an essential substrate of hyaluronan synthases (HAS), and further contributes to degrading the mRNA of HAS-2. Currently, several works support the idea that 4MU does not only act as an hyaluronan (HA) inhibitor(12,13). Indeed, our and other groups reported a direct effect of 4MU on CD44, RHAMM, MMPs, and some key signaling pathways(5,7,12–18). However, the effect of 4MU on metabolome and metabolic pathways is poorly described, and at least in GBM, there are no reports about it.

The metabolome constitutes the pool of metabolites inside cells, which is determined by cellular lineage and context(19). This context determines that pool's balance, and ultimately impairs cellular metabolism and behavior(20,21). In a tumor context, some metabolic pathways are enhanced, favoring tumor cell growth, migration, and invasion(22,23). Particularly in GBM, these characteristics are involved in the progression and malignancy of this type of tumor.

In the last decades, the use of nuclear magnetic resonance (NMR) to determine metabolites in several samples has been incresed(24,25). Particularly, NMR was widely used to determine bacteria and plant metabolites as well as metabolites in biological samples. However, the use of NMR to assess human cell extracts is not so extensive(26–29).

In this work, we performed NMR assays to determine the metabolite concentrations in the cellular extract of LN229 and U251 GBM cells under 4MU treatment and basal condition. Moreover, Metabolite set Quantitative Enrichment Analysis (QEA) was carried out to seek metabolic pathways modulated by 4MU in these cells. Also, we demonstrate the oxidative stress state induced by 4MU. Finally, we evaluate the N-glycosylation of both cell lines and the glycolytic state of U251 cells using a seahorse assay.

MATERIALS AND METHODS

Reagents

4-Methylumbelliferone (4MU) was purchased from Sigma-Aldrich (Saint Luis, Missouri, USA). Dihydrorodamine 123 (DHR), Höetch, DMEM, L-glutamine, streptomycin and penicillin were purchased

from Invitrogen (Waltham, Massachusetts, USA). Fetal bovine serum (FBS) was acquired from Internegocios, Argentina. Methanol was purchased from Cicarelli, Argentina.

Cell cultures

The LN229 and U251 human GBM cell lines (gently provided by Dr. Carolina Jancic) were grown in adherent cultures at 37°C in a 5% CO_2 atmosphere with DMEM supplemented with 10% heat-inactivated FBS, 2 mM L-glutamine, 100 µg/mL streptomycin and 100 IU/mL penicillin (DMEM-C) and tested for Mycoplasma every three months by DAPI staining and specific PCR. Cell passages of less than 20 were used for the described experiments.

Cell Treatments

For all assays, cells were seeded 24 h before treatment. Cells were treated with 4MU (0-1000 µM). Vehicle control cultures were also included. All incubations were performed at 37°C in a 5% CO_2 atmosphere.

Nuclear Magnetic Resonance (NMR)-based metabolomics

1×10^7cells were seeded in a 100 mm cell culture dish and treated with 1000 µM 4MU or with vehicle for 24 h. The cells were then centrifuged at 1500 rpm for 10 minutes, and the cell pellet was washed three times with phosphate-buffered saline (PBS). Following the washes, the cells were resuspended in 10 mL of ice-cold 80% methanol, disrupted by sonication, and centrifuged at 4 °C for 10 minutes at 14,000 × g. The resulting supernatants were collected and dried using a Savant SpeedVac concentrator (Thermo Scientific). The dried samples were reconstituted in 0.5 mL of sodium phosphate buffer prepared in D_2O (pH 7.40 ± 0.05), containing 3-trimethylsilyl-[2, 2, 3, 3, -$^2H_4$]-propionate (TSP) at a final concentration of 0.33 mM, and then transferred to 5 mm NMR tubes. All NMR measurements were carried out at 298 K on a Bruker Avance III spectrometer equipped with a proton resonance frequency of 600.1 MHz. The experimental protocols as well as data processing and analysis were performed in accordance with previously established methodologies(25,30).

Metabolite Quantification

For metabolite quantification only well-resolved, non-overlapping peaks of the identified metabolites were integrated. ^{1}H-NMR 1D spectra were acquired using a standard Bruker 1D NOESY pulse program with pre-saturation during relaxation delay and mixing time, and spoil gradients (noesygppr1d). To ensure over 99% magnetization recovery, an interpulse delay D1 of 10 s (>5 × T1) was applied. The signal area in the ¹H NMR spectrum is directly proportional to the molar concentration of the metabolites. The selected metabolites were quantified by integration, using both 0.33 mM of TSP as an internal standard and 10 mM of threonine as an external standard for absolute concentration determination. The concentration of each metabolite was determined using the following equation:

$$Cm = \frac{\Im \times Cstd \times Nstd}{Istd \times Nm}$$

In this equation, C_m denotes the concentration of the metabolite, I_m the integrated area of the metabolite resonance, N_m the number of protons contributing to that resonance, C_{std} corresponds to the concentration of the reference standard, I_{std} to the integral of the standard resonance, and N_{std} to the number of protons associated with the standard signal.

Differentially expressed metabolites (DEM)

A t-test was mapped robustly within each metabolite and between groups with the purrr R package, and the cut-off value was set at 0.05. Also, the dataset was group split; within both groups, each metabolite's mean and standard deviation (SD) of the abundance values were calculated. Subsequently, the mean abundance differences (Fold change) were computed for each metabolite with the pooled standard deviation, the square root of the sum of square SD (SD 4MU and SD Bas) divided by 2. The Cohen's effect size(31), the Fold Change divided by the pooled standard deviation was computed as a statistical effect size measurement, and the cut-off value was set at 80%.

Metabolite set Quantitative Enrichment Analysis (QEA)

The enrichment analysis was performed in the MetaboAnalyst 6.0 platform, which used package globaltest (32) (Jelle J. Goeman, Sara A. van de Geer, Floor de Kort and Hans C. van Houwelingen. A global test for groups of genes: testing association with a clinical outcome, Bioinformatics Vol. 20 no. 1 2004, pages 93-99). It uses a generalized linear model to estimate a Q-statistic for each metabolite set, which describes the correlation between compound concentration proles, X, and clinical outcomes, Y. The Q statistic for a metabolite set is the average of the Q statistics for each metabolite in the set.

The data processing pipeline includes standardizing compound labels with HMDB ID. Next, we selected the libraries of metabolic pathways associated with metabolite sets, particularly RaMP-DB (Pathway-based database), which includes 3,694 metabolite and lipid pathways, integrating KEGG via HMDB, Reactome, and WikiPathways(33–35). Also, we used libraries of disease-associated metabolite sets reported in human cerebral spinal fluid CFS, which includes 174 metabolites.

Lectin-binding Assay:

To determine protein N-glycosylation, binding to Concanavalin A (ConA) was studied by flow cytometry, as previously described (paper Oncotarget 2020 Gabri). Briefly, GBM cells were treated for 48 h prior to collection with enzyme-free cell dissociation buffer (Thermo Fisher Scientific, USA) and then washed with PBS. Biotinylated ConA (Vector Laboratories, USA) was incubated with fluorescein-streptavidin (Vector Laboratories, USA) in 1% Bovine Serum-Albumin (BSA) (Sigma, USA) in PBS on ice for 30 min.

Then, cells were incubated with the lectin-streptavidin complex on ice for 30 min. Acquisition was carried out by a FACSCalibur flow cytometer (Becton Dickinson, USA) and analyzed by Flowing software. Results are expressed as Median Fluorescence Intensity of events.

Seahorse Glycolysis Stress Test Assay:

To estimate the bioenergy function in U251 glioblastoma cells, $1.5x10^4$ U251 cells/100ul/well were seeded in a Seahorse cell culture miniplate in DMEM with 10% FBS and incubated for 24 h in CO2 incubator. After that, 4MU or vehicle treatment was added, and cells were incubated by additional 24 h. Following this, the culture media were washed and replaced with XF base media (DMEM plus 2mM Pyruvate, pH7,4) and incubated in a non-CO2 incubator for 1 h at 37 °C.

After that, the measurement of extracellular acidification rate (ECAR) was run after the injection of glycolysis agitating agents (100 mM glucose, 10 µM oligomycin and 500mM 2-deoxyglucose) at the drug injection ports respectively following 20 min of calibration and equilibration in the instrument. Oligomycin was mainly used to block mitochondrial respiration. Next, the recorded data were normalized concerning total cell using DAPI and nuclei counting. Agilent Seahorse XF24 analyzer permits to estimate the basal level of medium acidification, glycolysis medium acidification, maximum glycolytic capacity, glycolytic reserve and non-glycolytic medium acidification by using ECAR.

1,2,3-Dihydrorhodamine assay

$1x10^5$ cells/100 ul/well were seeded in a 96 well plate. After 24 h, 11ul of Höetch solution (1/1500) were added and cell were incubated for 30 min. After that, 50 ul of 1,2,3-Dihydrorhodamine (DHR) solution (1/1000) were added and plate was incubated 40 min more. Then, 60 ul of supernatant were discard and 100 ul of 2X treatment were added. After 1.5 h of incubation, plate was washed twice with PBS and representative photographs were taken using EVOS M7000 Imaging System. The number and intensity of positive cells were analyzed using Fiji software.

Statistical analysis.

Statistical significance was calculated using Prism 8 statistical software (Graph Pad Prism, San Diego, CA, USA). The data presented in this study is expressed as mean values ± SD if not otherwise stated. The letter “n” refers to the number of independently performed experiments corresponding to the data shown in each figure. This number was selected in each case considering the statistic test and the laboratory's capability, shown in the captions of each figure. Shapiro–Wilk´s normality test was performed before the statistical test. Levene's test analyzed the variances within each data group and was similar between the statistically compared groups. One-way ANOVA was used to compare three or more independent groups. The Student’s test (T-test) was performed to compare two independent groups, whereas for comparison of treated vs. untreated groups, Dunnet’s test was performed. Bonferroni’s test was used to make simultaneous multiple comparisons between different groups. P values < 0.05 were considered statistically significant.

The authors used a large language model (ChatGPT) to assist in improving the clarity and language of the manuscript. All scientific content, analysis, and conclusions were developed and verified by the authors.

RESULTS

Effect of 4MU on metabolites of GBM cells

To identify metabolic changes under 4MU treatment, U251, and LN229 cell lines were treated with 1000 µM 4MU or with the vehicle for 24 hours. After that we carried out untargeted ^{1}H-NMR metabolomics on methanol-extracted samples from cells. A total of 42 and 47 compounds were detected and identified in U251 and LN229 cells, respectively (Supplementary Table 1). A principal component analysis (PCA) and a partial least square-discriminant analysis (PLS-DA) were performed in order to detect the differences between treated and non-treated cells (**Figure 1 A and B)**. In the PCA, the two first principal components (PC) explained more than 70% of the total variation, clarifying the separation between groups.

Furthermore, to analyze the variation for each identified metabolite and visualize general grouping information, an Important features VIP values is shown **(Figure 1 C).**

Figure 1

4MU generates differentially expressed metabolites (DEM) on both cell lines.

Univariate statistical analyses were applied to seek Differential Expressed Metabolites (DEM) between 4MU and Vehicle groups. As shown in **Figure 2,** 4MU exerts changes in central metabolites in both cell lines. Even though in LN229 cells more metabolites were modified than in U251, in both cell lines 4MU diminished the concentration of NAD, a central bioenergetic metabolite. (**Figure 2 A and B,** respectively). Interestingly, 4MU augmented the concentration of NADP, a key co-factor related to Pentose Phosphate Metabolism, while decreased UDP-sugars on LN229 cells.

4MU impairs several metabolic pathways in both cell lines.

Metabolite set Quantitative Enrichment Analysis (QEA) was conducted in both U251 and LN229 cell lines under 4MU or vehicle treatment.The analysis reveals several metabolic pathways affected by 4MU treatment on U251 and LN229 cells. (**Figure 3 and 4,** respectively).

Interestingly, in both cell lines, the metabolites and lipid pathways affected by treatment are related to proteoglycan and glycolipids synthesis and metabolism, as well as protein N-glycosylation.

Related to the KEEG database, the metabolic pathways affected by 4MU with a greater or minor relevance majorly appear modulated in both cell lines. Interestingly, this analysis reinforces the idea that 4MU impairs pathways implicated in the glycosylation of several molecules, and it makes the bioenergetic pathways appear to be the most affected.

4MU enhances the oxidative stress on both cell lines.

Considering that 4MU affected the NAD levels in both cell lines and that this metabolite is closely related to oxidative stress protection, we performed a DHR assay to evaluate the cell redox state. As shown in **Figure 5 A**, after 1.5 h of treatment, 4MU enhanced the signal of DHR in both cell lines, reinforcing the idea that treatment with 4MU induces an oxidative stress state. Below the graph, representative microphotographs from one assay are shown for each cell line (**Figure 5 B**).

4MU alters the glycosylation pattern on both cell lines.

In view of 4MU modulation of several glycosylation pathways on both cell lines, we performed lectin binding assay and flow cytometry to evaluate the changes in the protein glycosylation pattern under 4MU treatment. We compared the glycan profile considering the binding to the lectin Concanavalin A (ConA) and Phytohemagglutinin-E (PHA-E) on U251 and LN229 cells. ConA recognizes oligomannose-type N-glycans with high-affinity and complex-type bi-antennary N-glycans with low-affinity, while PHA-E binds to structures with β1,6-GlcNAc branches of complex tri- and tetra-antennary N-glycans.

As shown in **Figure 6**, 4MU modulates ConA and PHA-E binding, suggesting that the expression of N-glycans is altered on U251 **(A)** and LN229 **(B)** cells under 4MU treatment.

4MU affects the glycolysis rate in U251 cells

Considering that several glucose metabolic pathways were found affected by 4MU on both cell lines, we evaluated energetic metabolism by a Seahorse Glycolysis Stress Test Assay on U251 cells. We evaluated cellular ECARs in U251 cells under 4MU treatment to evaluate the potential activity of 4MU in regulating cell bioenergetics. As shown in **Figure 7**, the overall ECARs of U251 were increased under 4MU treatment **(A)**. We further assessed ECAR indexes and found both basal glycolysis and glycolytic capacity were notably increased in 4MU-treated U251 cells (**B**).

DISCUSSION

As described in the Introduction section, GBM is the most common and aggressive tumor of CNS in adults. The fact that 50% of patients are refractory to chemotherapy highlights the necessity of new alternatives drugs. In this scenario, in our lab, we described the anti-tumor effects of 4MU, a coumarin derivative without adverse effects reported. Although the effect of 4MU on hyaluronan synthesis is clear and there is enough evidence about its HA-independent effect, the underlying mechanisms of action and the molecules involved remain unknown.

As shown in the previous section, the treatment with 4MU induces an early oxidative stress response in glioblastoma cells, detectable at 1.5 hours, as demonstrated by the increase in DHR signal. This redox imbalance could be the primary trigger of the subsequent metabolic alterations observed at 24 hours, characterized by glycolysis enhancement in U251 and NAD decreasing in both cell lines. For LN229 cells, the NAD diminish was also accompanied by a decrease in UDP-Glucose and UDP-glucoronate and an

augment in NADP. This initial state is followed by an altered N-glycosylation on both cell lines, revealed both by ConA and PHA-L binding.

Interestingly, we found that 4MU decreased the levels of NAD+ in both cell lines. This metabolite is essential to DNA repair as well as oxidative stress resistance, which led to its proposal as an anti-cancer therapeutic target several years ago. NAD depletion may be the result of the cells' damage response to ROS increase, specifically enhanced DNA repair processes mediated by the PARP protein family that uses NAD as a cofactor, which leads to inhibition of sirtuins by NAD+ decrease, ultimately leading to cell senescence (36–38). Also, NAD reduction may reflect exhaustion of essential cofactors for redox and glycolytic reactions, compromising the cells' ability to maintain normal energy metabolism in cancer in general and particularly in GBM (39–42).

In cancer cells, metabolism is redirected to glycolysis to enhance the production of metabolic compounds employed by cancer cells in proliferation and growth. In this work, we observed that 4MU enhanced the glycolytic state of U251 cells. This 4MU effect could be linked to its known mechanism of HA synthesis inhibition by depleting cytosolic UDP-Glucuronate and UDP-GlcNAc pools, as reflected by the metabolomics studies in both cell lines. This could lead to an accumulation of glycolysis substrates, which increases glycolysis flux, as reported by Grandoch *et al* in brown adipose tissue models (43). This mechanism causes a further increase in reactive oxygen species (ROS), which could lead to cell death. However, several cancer types overcome the problem generated by ROS augment by increasing the antioxidant machinery (44). Further studies are yet to be conducted to determine if this is the initial step that leads to the rise in ROS or if there are other mechanisms involved. Considering the NAD depletion, the increase in glycolysis measured by Seahorse may also be a compensatory mechanism to maintain ATP production despite ROS increase and NAD reduction, while the ROS rise indicates a redox imbalance that could contribute to cellular damage (45). This pattern aligns with the altered metabolism of glioblastomas, which rely on glycolysis and show resistance to oxidative stress (46). Furthermore, NADP increasing suggests activation of antioxidant pathways such as the pentose phosphate pathway, generating reducing power necessary to neutralize accumulated ROS (47).

On the other hand, the drop in UDP-Glucose, UDP-Glucuronate, and UDP-GlcNAc reflects a glycosylation deficit, affecting the synthesis of glycosylated proteins and lipids, potentially impacting cellular signaling and stability (48,49). Moreover, through Metabolite Set Enrichment Analyses we found that 4MU impairs N-glycosylation pathways and by ConA and PHA-L binding assays we corroborated that 4MU altered N-glycosylation on both cell lines. It is worth noting that in the LN229 cell line, where a marked decrease in the metabolites UDP-metabolites were observed, we can also see a significant reduction in the different glycosylated structures that were evaluated in parallel , as these metabolites are the necessary precursors for N-glycosylation.

At 48 hours, the sustained alteration in N-glycosylation, together with the previously reported senescence induction, suggests that cells are unable to reverse the initial metabolic stress, activating cell cycle arrest programs(5,50).

Overall, these findings suggest that 4MU treatment first induces oxidative stress in glioblastoma cells, which then drives downstream metabolic and N-glycosylation alterations that, if persistent, culminate in cellular senescence. This underscores the importance of the temporal sequence linking oxidative stress, energy metabolism, glycosylation, and cell fate decisions, with implications for therapeutic strategies targeting metabolic vulnerabilities in this tumor type (39,49,51,52).

CONCLUSION

The treatment with 4MU induces oxidative stress in glioblastoma cells as early as 1.5 hours, preceding broader metabolic alterations. If sustained, this leads to functional consequences such as induction of cellular senescence and altered N-glycosylation, reflecting a potentially cytostatic effect of 4MU and providing a pathway for possible therapeutic interventions.

Abbreviations

4MU: 4-Methylumbelliferone

BSA: Bovine Serum-Albumin

ConA: Concanavalin A

DEM: Differentially expressed metabolites

DHR: dihydrorhodamine

ECAR: Extracellular acidification rate

GBM: Glioblastoma

HA: Hyaluronan

HAS: Hyaluronan synthases

NMR: Nuclear magnetic resonance

PBS: Phosphate-buffered saline

PC: Principal components

PCA: Principal component analysis

PHA-E: Phytohemagglutinin-E

PLS-DA: Partial least square-discriminant analysis

QEA: quantitative enrichment analysis

SD: Standard deviation

TSP: 3-trimethylsilyl-[2, 2, 3, 3, -$^{2}H_{4}$]-propionate

Declarations

Ethics approval and consent to participate

Not applicable

Consent for publication

Not applicable

Availability of data and materials

The datasets used and/or analysed during the current study are available from the corresponding author on reasonable request.

Competing interests

The authors declare that they have no competing interests

Funding

This work was supported by Consejo Nacional de Investigaciones Científicas y Técnicas, CONICET - PIP N°0303 [Silvina Lompardia], Universidad de Buenos Aires - UBACYT 20020170100454BA [Silvia Hajos and Silvina Lompardia] and, Agencia Nacional de Promoción Científica y Tecnológica, PICT-2021-GRFTI-00074 [Lompardía Silvina], PICT-2021-I-INVI-00295 [Pibuel Matías].

Authors' contributions

DP and MAP performed the experiments and figures, analysed the data and wrote the manuscript. DP, MML and LP performed the experiments, analysed the data and wrote the manuscript. SEH, MG and MA contributed to the design of the study and editing the manuscript. NS, FN and MF collaborated with the experimental design. PG and CM collaborated editing manuscript. SLL contributed to the design of the study. MAP supervised the work. All authors contributed to the work and have read and approved the final manuscript.

Acknowledgements

We are grateful to Consejo Nacional de Investigaciones Científicas y Técnicas, Universidad de Buenos Aires and Agencia Nacional de Promoción Científica y Tecnológica for providing the funding that supported this work and to Celnova Pharma for providing temozolomide.

References

1. Czarnywojtek A, Borowska M, Dyrka K, Van Gool S, Sawicka-Gutaj N, Moskal J, et al. Glioblastoma Multiforme: The Latest Diagnostics and Treatment Techniques. Pharmacology [Internet]. 2023 Sep 1 [cited 2025 Aug 18];108(5):423–31. Available from: https://pubmed.ncbi.nlm.nih.gov/37459849/
2. Jezierzański M, Nafalska N, Stopyra M, Furgoł T, Miciak M, Kabut J, et al. Temozolomide (TMZ) in the Treatment of Glioblastoma Multiforme—A Literature Review and Clinical Outcomes. Curr Oncol [Internet]. 2024 Jul 1 [cited 2025 Aug 18];31(7):3994–4002. Available from: https://pubmed.ncbi.nlm.nih.gov/39057168/
3. Louis DN, Perry A, Wesseling P, Brat DJ, Cree IA, Figarella-Branger D, et al. The 2021 WHO classification of tumors of the central nervous system: A summary. Neuro Oncol [Internet]. 2021 Aug 1 [cited 2023 Jan 9];23(8):1231–51. Available from: https://pubmed.ncbi.nlm.nih.gov/34185076/
4. Tomar MS, Kumar A, Srivastava C, Shrivastava A. Elucidating the mechanisms of Temozolomide resistance in gliomas and the strategies to overcome the resistance. Biochim Biophys acta Rev cancer [Internet]. 2021 Dec 1 [cited 2023 Jan 9];1876(2). Available from: https://pubmed.ncbi.nlm.nih.gov/34419533/
5. Pibuel M, Poodts D, Díaz M, Molinari Y, Franco P, Hajos S, et al. Antitumor effect of 4MU on glioblastoma cells is mediated by senescence induction and CD44, RHAMM and p-ERK modulation. Cell death Discov [Internet]. 2021 Dec 9 [cited 2021 Oct 14];7(1):280. Available from: https://pubmed.ncbi.nlm.nih.gov/34628469/
6. Pibuel M, Poodts D, Sias S, Byrne A, Hajos S, Franco P, et al. 4-Methylumbelliferone enhances the effects of chemotherapy on both temozolomide-sensitive and resistant glioblastoma cells. Sci Rep. 2023;1(9356).
7. Pibuel MA, Díaz M, Molinari Y, Poodts D, Silvestroff L, Lompardía SL, et al. 4-Methylumbelliferone as a potent and selective antitumor drug on a glioblastoma model. Glycobiology [Internet]. 2021 Jan 1 [cited 2020 Jun 17];31(1):29–43. Available from: https://pubmed.ncbi.nlm.nih.gov/32472122/
8. Nagy N, Kuipers HF, Frymoyer AR, Ishak HD, Bollyky JB, Wight TN, et al. 4-Methylumbelliferone treatment and hyaluronan inhibition as a therapeutic strategy in inflammation, autoimmunity, and cancer. Front Immunol [Internet]. 2015 [cited 2020 Apr 14];6(MAR):123. Available from: http://www.ncbi.nlm.nih.gov/pubmed/25852691
9. Kuipers HF, Nagy N, Ruppert SM, Sunkari VG, Marshall PL, Gebe JA, et al. The pharmacokinetics and dosing of oral 4-methylumbelliferone for inhibition of hyaluronan synthesis in mice. Clin Exp Immunol. 2016;
10. Rosser JI, Nagy N, Goel R, Kaber G, Demirdjian S, Saxena J, et al. Oral hymecromone decreases hyaluronan in human study participants. J Clin Invest [Internet]. 2022 May 2 [cited 2023 Jan 9];132(9). Available from: https://pubmed.ncbi.nlm.nih.gov/35499083/
11. Chen X, Li H, Deng Y, Meng J, Zhao S, Wooton-Kee CR, et al. The potential of 4-Methylumbelliferone to be repurposed for treating liver fibrosis. Biomed Pharmacother [Internet]. 2025 Sep 1 [cited 2025

Aug 18];190. Available from: https://pubmed.ncbi.nlm.nih.gov/40774020/

12. Karalis TTTT, Heldin P, Vynios DDHD, Neill T, Buraschi S, Iozzo RR V., et al. Tumor-suppressive functions of 4-MU on breast cancer cells of different ER status: Regulation of hyaluronan/HAS2/CD44 and specific matrix effectors. Matrix Biol. 2019;78(78–79):118–38.
13. Ishizuka S, Askew EB, Ishizuka N, Knudson CB, Knudson W. 4-Methylumbelliferone diminishes catabolically activated articular chondrocytes and cartilage explants via a mechanism independent of hyaluronan inhibition. J Biol Chem. 2016;291(23):12087–104.
14. Lompardía SL, Papademetrio DL, Mascaró M, Del Carmen Álvarez EM, Hajos SE. Human leukemic cell lines synthesize hyaluronan to avoid senescence and resist chemotherapy. Glycobiology. 2013;23(12):1463–76.
15. Lompardía SL, Díaz M, Papademetrio DLDL, Pibuel M, Álvarez É, Hajos SESESE. 4-methylumbelliferone and imatinib combination enhances senescence induction in chronic myeloid leukemia cell lines. Invest New Drugs [Internet]. 2017 Feb 1 [cited 2020 Apr 14];35(1):1–10. Available from: http://www.ncbi.nlm.nih.gov/pubmed/27718039
16. Fedorova V V., Tsitrina A, Halimani N, Kotelevtsev Y V. 4-Methylumbelliferone, an Inhibitor of Hyaluronan Synthase, Prevents the Development of Oncological, Inflammatory, Degenerative, and Autoimmune Diseases. Biochem [Internet]. 2025 Jan 1 [cited 2025 Aug 18];90(1):1–18. Available from: https://pubmed.ncbi.nlm.nih.gov/40058970/
17. Liu M, Tolg C, Turley E, Turley E. Dissecting the Dual Nature of Hyaluronan in the Tumor Microenvironment. Front Immunol. 2019;10(May):1–9.
18. Terabe K, Ohashi Y, Tsuchiya S, Ishizuka S, Knudson CB, Knudson W. Chondroprotective effects of 4-methylumbelliferone and hyaluronan synthase-2 overexpression involve changes in chondrocyte energy metabolism. J Biol Chem [Internet]. 2019 Nov 22 [cited 2023 Jan 9];294(47):17799–817. Available from: https://pubmed.ncbi.nlm.nih.gov/31619518/
19. Zhang A, Sun H, Xu H, Qiu S, Wang X. Cell metabolomics. Omi A J Integr Biol [Internet]. 2013 Oct 1 [cited 2025 Aug 18];17(10):495–501. Available from: https://pubmed.ncbi.nlm.nih.gov/23988149/
20. Gebregiworgis T, Powers R. Application of NMR Metabolomics to Search for Human Disease Biomarkers. Comb Chem High Throughput Screen [Internet]. 2012 Sep 4 [cited 2025 Aug 18];15(8):595–610. Available from: https://pubmed.ncbi.nlm.nih.gov/22480238/
21. Newgard CB. Metabolomics and Metabolic Diseases: Where Do We Stand? Cell Metab [Internet]. 2017 Jan 10 [cited 2025 Aug 18];25(1):43–56. Available from: https://pubmed.ncbi.nlm.nih.gov/28094011/
22. Suri GS, Kaur G, Carbone GM, Shinde D. Metabolomics in oncology. Cancer Rep [Internet]. 2023 Mar 1 [cited 2025 Aug 18];6(3). Available from: https://pubmed.ncbi.nlm.nih.gov/36811317/
23. Schmidt DR, Patel R, Kirsch DG, Lewis CA, Vander Heiden MG, Locasale JW. Metabolomics in cancer research and emerging applications in clinical oncology. CA Cancer J Clin [Internet]. 2021 Jul [cited 2025 Aug 18];71(4):333–58. Available from: https://pubmed.ncbi.nlm.nih.gov/33982817/

24. Moco S. Studying Metabolism by NMR-Based Metabolomics. Front Mol Biosci [Internet]. 2022 Apr 27 [cited 2024 Mar 21];9. Available from: /pmc/articles/PMC9094115/
25. Pellizza L, Bialer MG, Sieira R, Aran M. MliR, a novel MerR-like regulator of iron homeostasis, impacts metabolism, membrane remodeling, and cell adhesion in the marine Bacteroidetes Bizionia argentinensis. Front Microbiol [Internet]. 2022 Sep 2 [cited 2024 Mar 21];13. Available from: /pmc/articles/PMC9478572/
26. Letertre MPM, Giraudeau P, de Tullio P. Nuclear Magnetic Resonance Spectroscopy in Clinical Metabolomics and Personalized Medicine: Current Challenges and Perspectives. Front Mol Biosci [Internet]. 2021 Sep 20 [cited 2024 Mar 21];8. Available from: https://pubmed.ncbi.nlm.nih.gov/34616770/
27. Ranjan R, Sinha N. Nuclear magnetic resonance (NMR)-based metabolomics for cancer research. NMR Biomed [Internet]. 2019 Oct 1 [cited 2024 Mar 21];32(10). Available from: https://pubmed.ncbi.nlm.nih.gov/29733484/
28. Pienkowski T, Kowalczyk T, Garcia-Romero N, Ayuso-Sacido A, Ciborowski M. Proteomics and metabolomics approach in adult and pediatric glioma diagnostics. Biochim Biophys acta Rev cancer [Internet]. 2022 May 1 [cited 2024 Mar 21];1877(3). Available from: https://pubmed.ncbi.nlm.nih.gov/35304294/
29. Zhao K, Calero-Pérez P, Bopp MHA, Möschl V, Pagenstecher A, Mulero-Acevedo M, et al. Correlation of MR-Based Metabolomics and Molecular Profiling in the Tumor Microenvironment of Temozolomide-Treated Orthotopic GL261 Glioblastoma in Mice. Int J Mol Sci [Internet]. 2023 Dec 1 [cited 2024 Mar 21];24(24). Available from: https://pubmed.ncbi.nlm.nih.gov/38139457/
30. Avalos JC, Pellizza L, Aran M. Metabolic alterations associated with epileptic seizures detected by NMR spectroscopy. Sci Rep [Internet]. 2025 Dec 1 [cited 2025 Oct 13];15(1). Available from: https://pubmed.ncbi.nlm.nih.gov/40781139/
31. Cohen J. Statistical power analysis for the behavioral sciences (2nd ed.). Hillsdale, NJ: Lawrence Earlbaum Associates. Lawrence Earlbaum Assoc. 1988;286.
32. Goeman JJ, Van de Geer S, De Kort F, van Houwellingen HC. A global test for groups of genes: testing association with a clinical outcome. Bioinformatics [Internet]. 2004 Jan 1 [cited 2025 Dec 9];20(1):93–9. Available from: https://dx.doi.org/10.1093/bioinformatics/btg382
33. Kanehisa M, Furumichi M, Sato Y, Matsuura Y, Ishiguro-Watanabe M. KEGG: biological systems database as a model of the real world. Nucleic Acids Res [Internet]. 2025 Jan 6 [cited 2026 Jun 22];53(D1):D672–7. Available from: https://pubmed.ncbi.nlm.nih.gov/39417505/
34. Kanehisa M. Toward understanding the origin and evolution of cellular organisms. Protein Sci [Internet]. 2019 Nov 1 [cited 2026 Jun 22];28(11):1947–51. Available from: https://pubmed.ncbi.nlm.nih.gov/31441146/
35. Kanehisa M, Goto S. KEGG: kyoto encyclopedia of genes and genomes. Nucleic Acids Res [Internet]. 2000 Jan 1 [cited 2026 Jun 22];28(1):27–30. Available from: https://pubmed.ncbi.nlm.nih.gov/10592173/

36. Mogol AN, Kaminsky AZ, Dutton DJ, Erdogan ZM. Targeting NAD+ Metabolism: Preclinical Insights into Potential Cancer Therapy Strategies. Endocrinol (United States) [Internet]. 2024 May 1 [cited 2025 Aug 14];165(5). Available from: https://pubmed.ncbi.nlm.nih.gov/38565429/
37. Massudi H, Grant R, Guillemin GJ, Braidy N. NAD + metabolism and oxidative stress: The golden nucleotide on a crown of thorns. Redox Rep [Internet]. 2012 Jan [cited 2025 Aug 14];17(1):28–46. Available from: https://pubmed.ncbi.nlm.nih.gov/22340513/
38. Chmielewski JP, Bowlby SC, Wheeler FB, Shi L, Sui G, Davis AL, et al. CD38 inhibits prostate cancer metabolism and proliferation by reducing cellular NAD+ pools. Mol Cancer Res [Internet]. 2018 Nov 1 [cited 2025 Aug 14];16(11):1687–700. Available from: https://pubmed.ncbi.nlm.nih.gov/30076241/
39. Kennedy BE, Sharif T, Martell E, Dai C, Kim Y, Lee PWK, et al. NAD+ salvage pathway in cancer metabolism and therapy. Pharmacol Res [Internet]. 2016 Dec 1 [cited 2025 Aug 14];114:274–83. Available from: https://pubmed.ncbi.nlm.nih.gov/27816507/
40. Navas LE, Carnero A. NAD+ metabolism, stemness, the immune response, and cancer. Signal Transduct Target Ther [Internet]. 2021 Dec 1 [cited 2025 Aug 14];6(1). Available from: https://pubmed.ncbi.nlm.nih.gov/33384409/
41. Tateishi K, Wakimoto H, Iafrate AJ, Tanaka S, Loebel F, Lelic N, et al. Extreme Vulnerability of IDH1 Mutant Cancers to NAD+ Depletion. Cancer Cell [Internet]. 2015 Dec 14 [cited 2025 Aug 14];28(6):773–84. Available from: https://pubmed.ncbi.nlm.nih.gov/26678339/
42. Lee M, Yoo JH, Kim I, Kang S, Lee W, Kim S, et al. The compartment-specific manipulation of the NAD+/NADH ratio affects the metabolome and the function of glioblastoma. Sci Rep [Internet]. 2024 Dec 1 [cited 2025 Aug 14];14(1). Available from: https://pubmed.ncbi.nlm.nih.gov/39232046/
43. Grandoch M, Flögel U, Virtue S, Maier JK, Jelenik T, Kohlmorgen C, et al. 4-Methylumbelliferone improves the thermogenic capacity of brown adipose tissue. Nat Metab [Internet]. 2019 May 1 [cited 2025 Dec 3];1(5):546–59. Available from: https://pubmed.ncbi.nlm.nih.gov/31602424/
44. Mossenta M, Busato D, Dal Bo M, Toffoli G. Glucose metabolism and oxidative stress in hepatocellular carcinoma: Role and possible implications in novel therapeutic strategies. Cancers (Basel) [Internet]. 2020 Jun 1 [cited 2025 Aug 18];12(6):1–30. Available from: https://pubmed.ncbi.nlm.nih.gov/32585931/
45. Schieber M, Chandel NS. ROS function in redox signaling and oxidative stress. Curr Biol [Internet]. 2014 May 19 [cited 2025 Aug 18];24(10). Available from: https://pubmed.ncbi.nlm.nih.gov/24845678/
46. Agrawal K, Asthana S, Kumar D. Role of Oxidative Stress in Metabolic Reprogramming of Brain Cancer. Cancers (Basel) [Internet]. 2023 Oct 1 [cited 2025 Aug 18];15(20). Available from: https://pubmed.ncbi.nlm.nih.gov/37894287/
47. Trejo-Solís C, Escamilla-Ramírez Á, Gómez-Manzo S, Castillo-Rodriguez RA, Palomares-Alonso F, Castillo-Pérez C, et al. The pentose phosphate pathway (PPP) in the glioma metabolism: A potent

enhancer of malignancy. Biochimie [Internet]. 2025 May 1 [cited 2025 Aug 18];232:117–26. Available from: https://pubmed.ncbi.nlm.nih.gov/39894336/

48. Akella NM, Ciraku L, Reginato MJ. Fueling the fire: Emerging role of the hexosamine biosynthetic pathway in cancer. BMC Biol [Internet]. 2019 Jul 4 [cited 2025 Aug 18];17(1). Available from: https://pubmed.ncbi.nlm.nih.gov/31272438/
49. Schjoldager KT, Narimatsu Y, Joshi HJ, Clausen H. Global view of human protein glycosylation pathways and functions. Nat Rev Mol Cell Biol [Internet]. 2020 Dec 1 [cited 2025 Aug 18];21(12):729–49. Available from: https://pubmed.ncbi.nlm.nih.gov/33087899/
50. Campisi J. Aging, Cellular Senescence, and Cancer. Annu Rev Physiol [Internet]. 2013;75(1):685–705. Available from: http://www.annualreviews.org/doi/10.1146/annurev-physiol-030212-183653
51. Covarrubias AJ, Perrone R, Grozio A, Verdin E. NAD+ metabolism and its roles in cellular processes during ageing. Nat Rev Mol Cell Biol [Internet]. 2021 Feb 1 [cited 2025 Aug 18];22(2):119–41. Available from: https://pubmed.ncbi.nlm.nih.gov/33353981/
52. Vlashi E, Lagadec C, Vergnes L, Matsutani T, Masui K, Poulou M, et al. Metabolic state of glioma stem cells and nontumorigenic cells. Proc Natl Acad Sci U S A [Internet]. 2011 Oct 20 [cited 2025 Aug 18];108(38):16062–7. Available from: https://pubmed.ncbi.nlm.nih.gov/21900605/

Figures

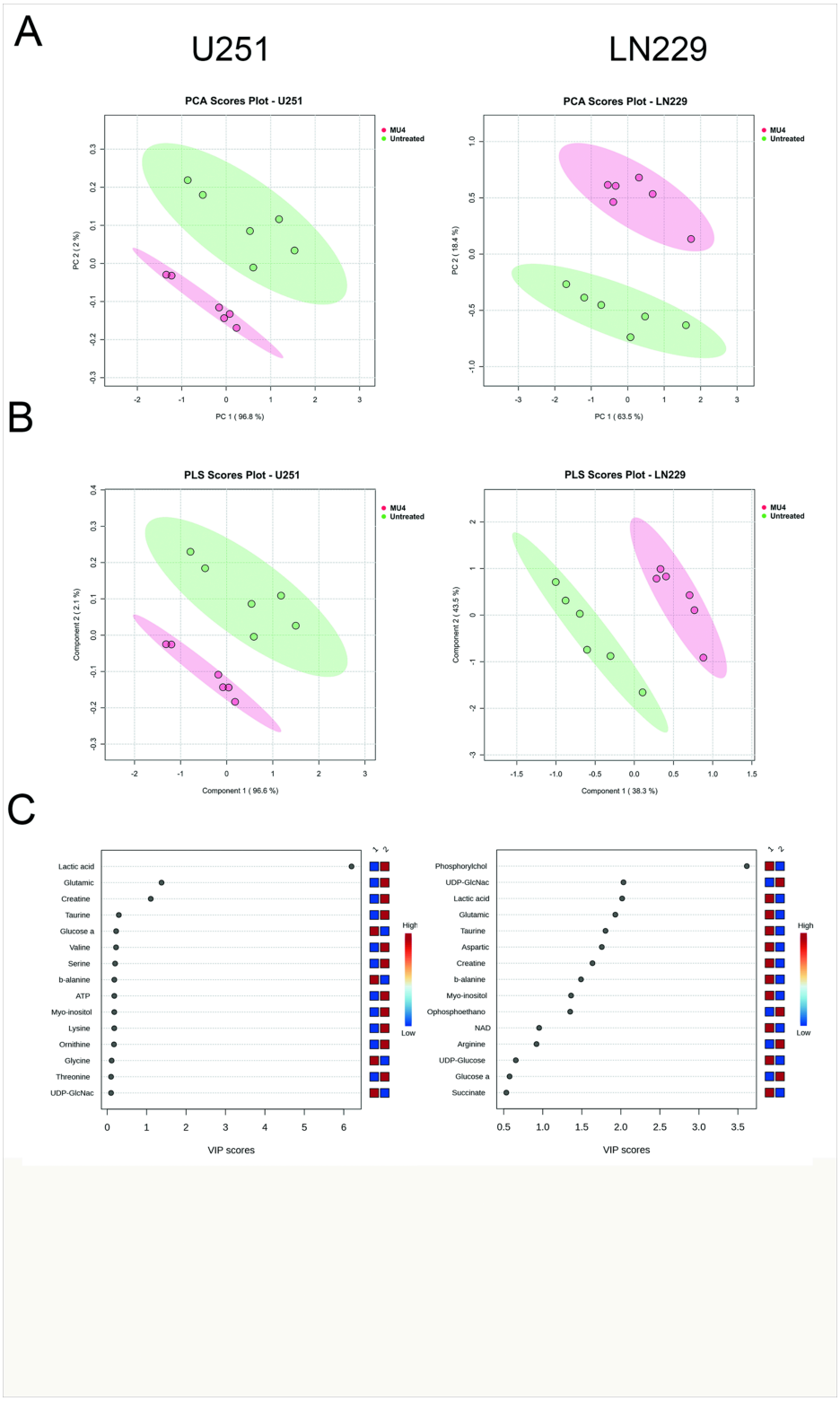


Figure 1

4MU effects on GBM cells' metabolites revealed by NMR metabolomics. **(A)** Plot for the first principal components under Principal component analysis (PCA) and (**B**) Partial least square-discriminant analysis (PLS-DA) of 4MU-treated and untreated GBM cells. (**C**) Main metabolites variation under Important features VIP values analysis.

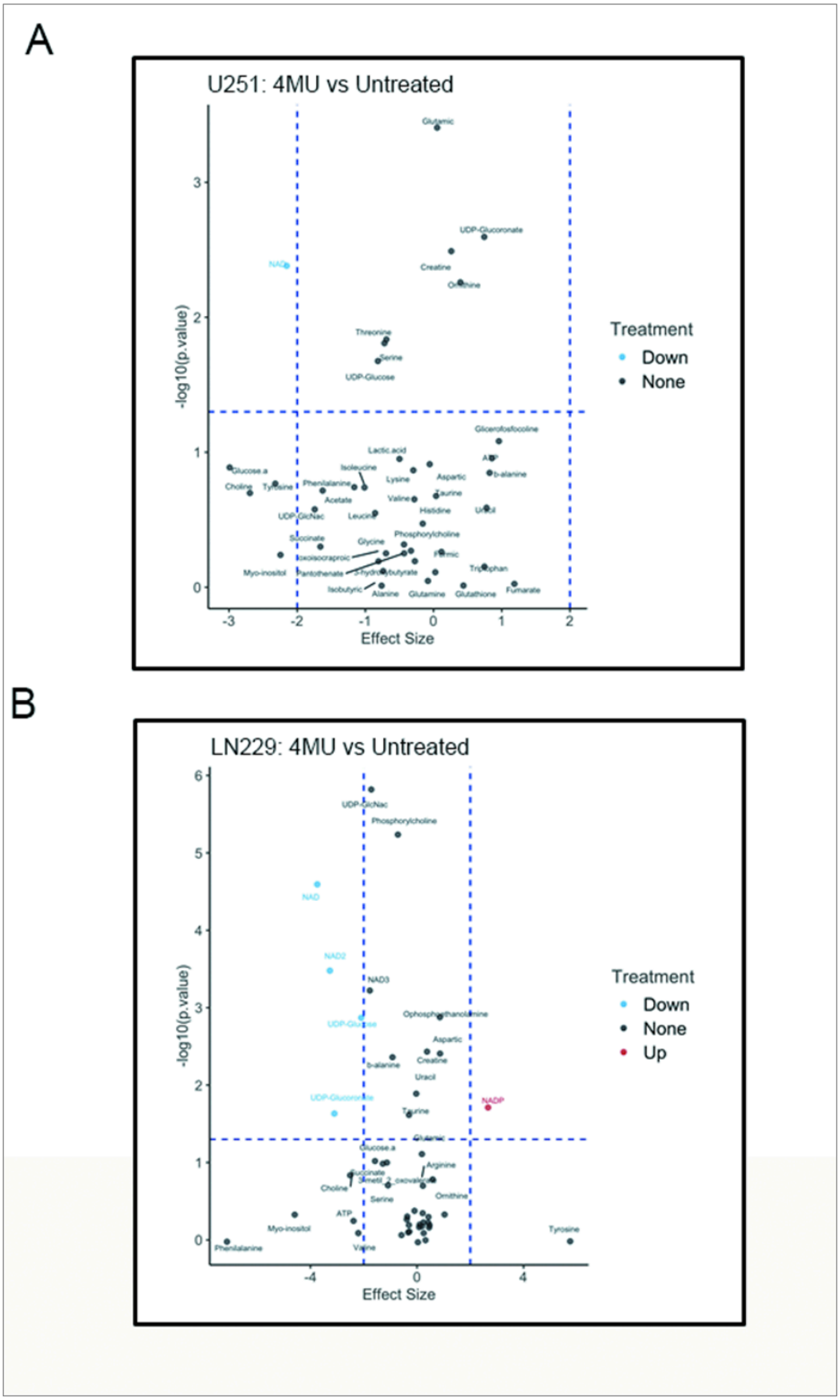


Figure 2

Differentially expressed metabolites in (**A**) U251 and (**B**) LN229 cells under 4MU treatment, following NMR-based metabolomics and univariate statistical analysis.

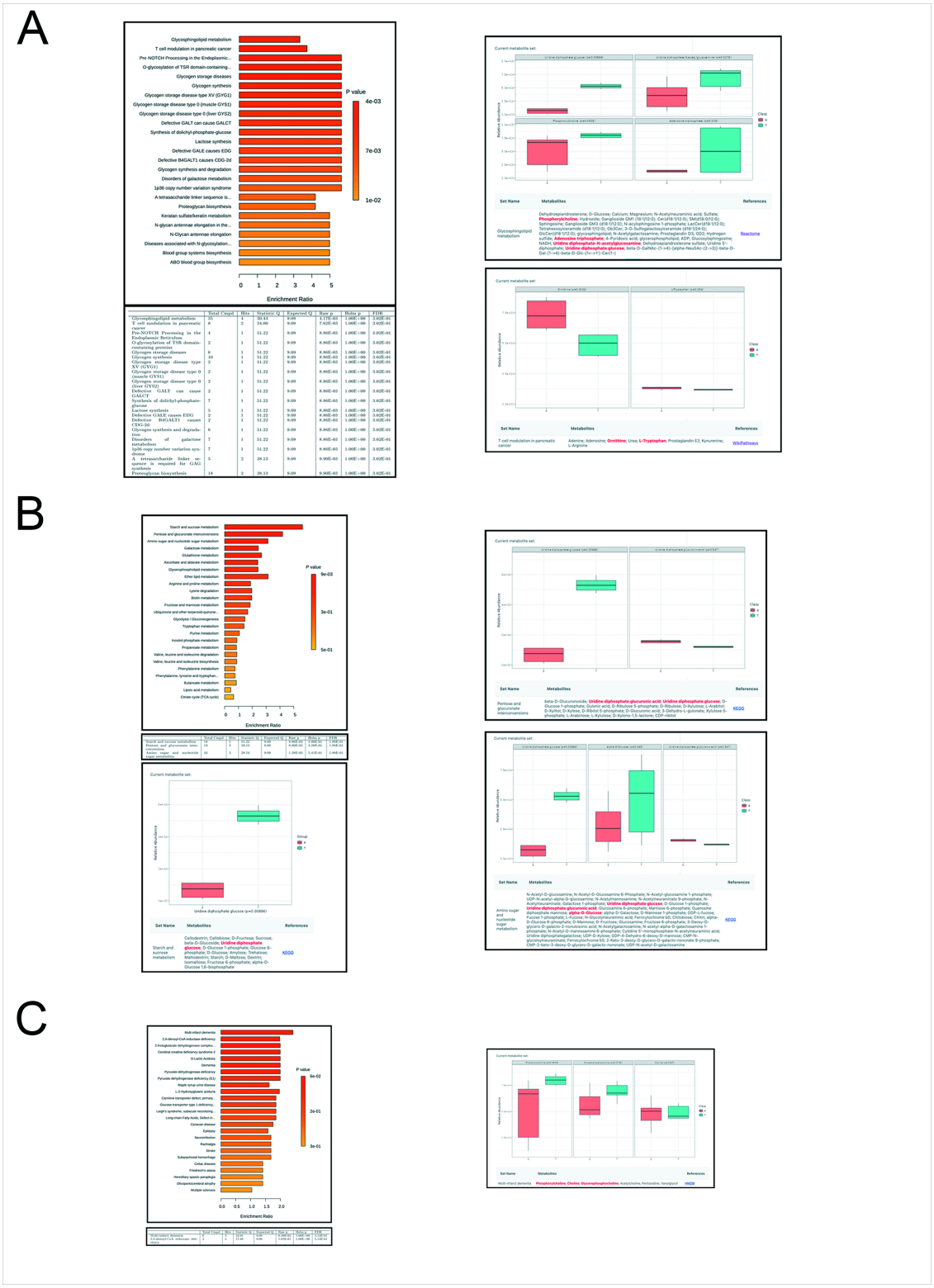


Figure 3

Metabolite set Quantitative Enrichment Analysis (QEA) of U251 cells under treatment with 4MU. (A) QEA using RaMP-DB (Pathway-based database, integrating KEGG via HMDB, Reactome, WikiPathways). (B) QEA using KEEG (Pathway-based database, integrating KEGG based on human metabolic pathways). (C) QEA using CFS (Disease signature metabolite sets reported in human cerebral spinal fluid (CSF).

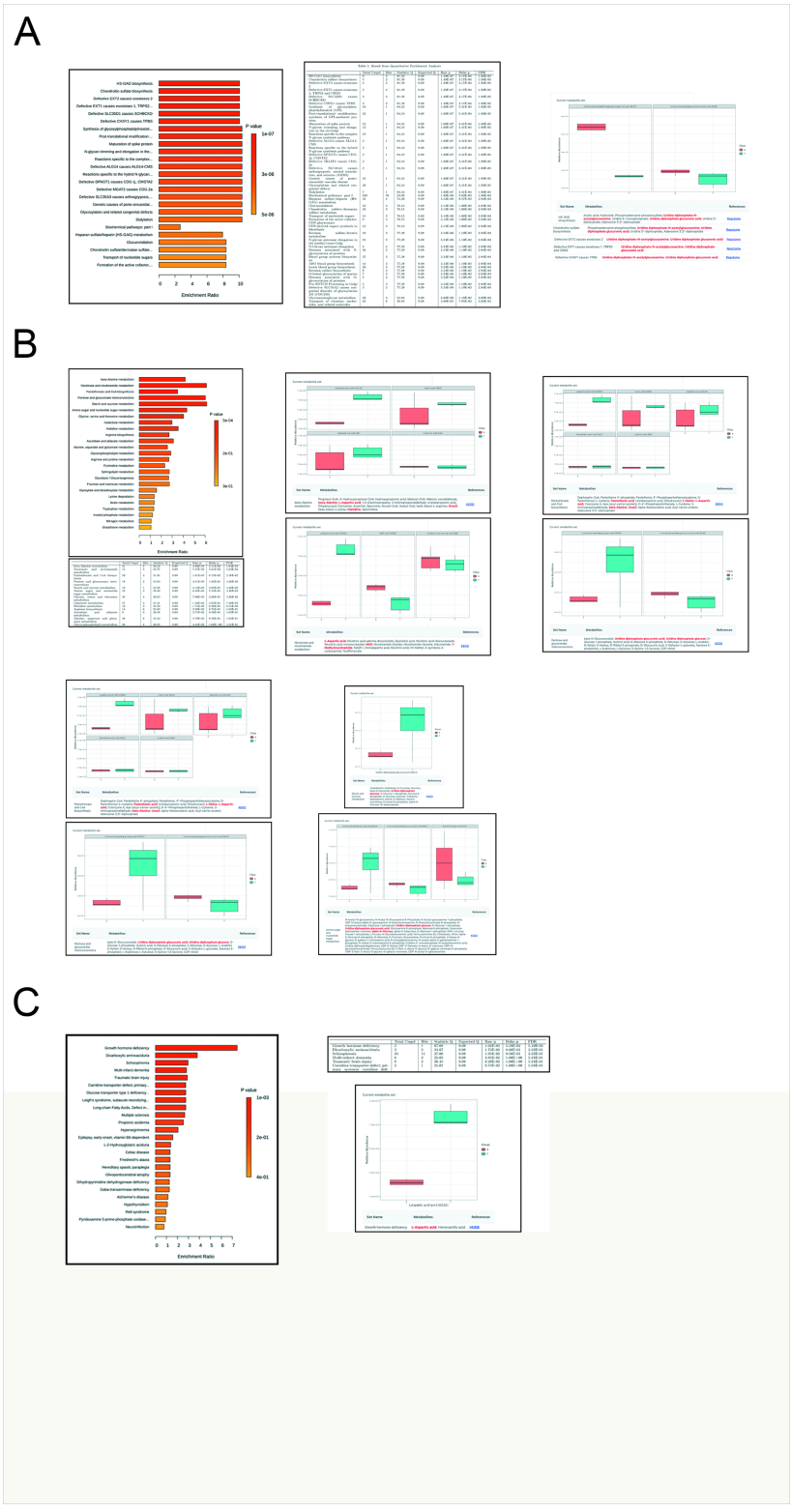


Figure 4

Metabolite set Quantitative Enrichment Analysis (QEA) of LN229 cells under treatment with 4MU. (A) QEA using RaMP-DB (Pathway-based database, integrating KEGG via HMDB, Reactome, WikiPathways). (B) QEA using KEEG (Pathway-based database, integrating KEGG based on human metabolic pathways). (C) QEA using CFS (Disease signature metabolite sets reported in human cerebral spinal fluid (CSF).

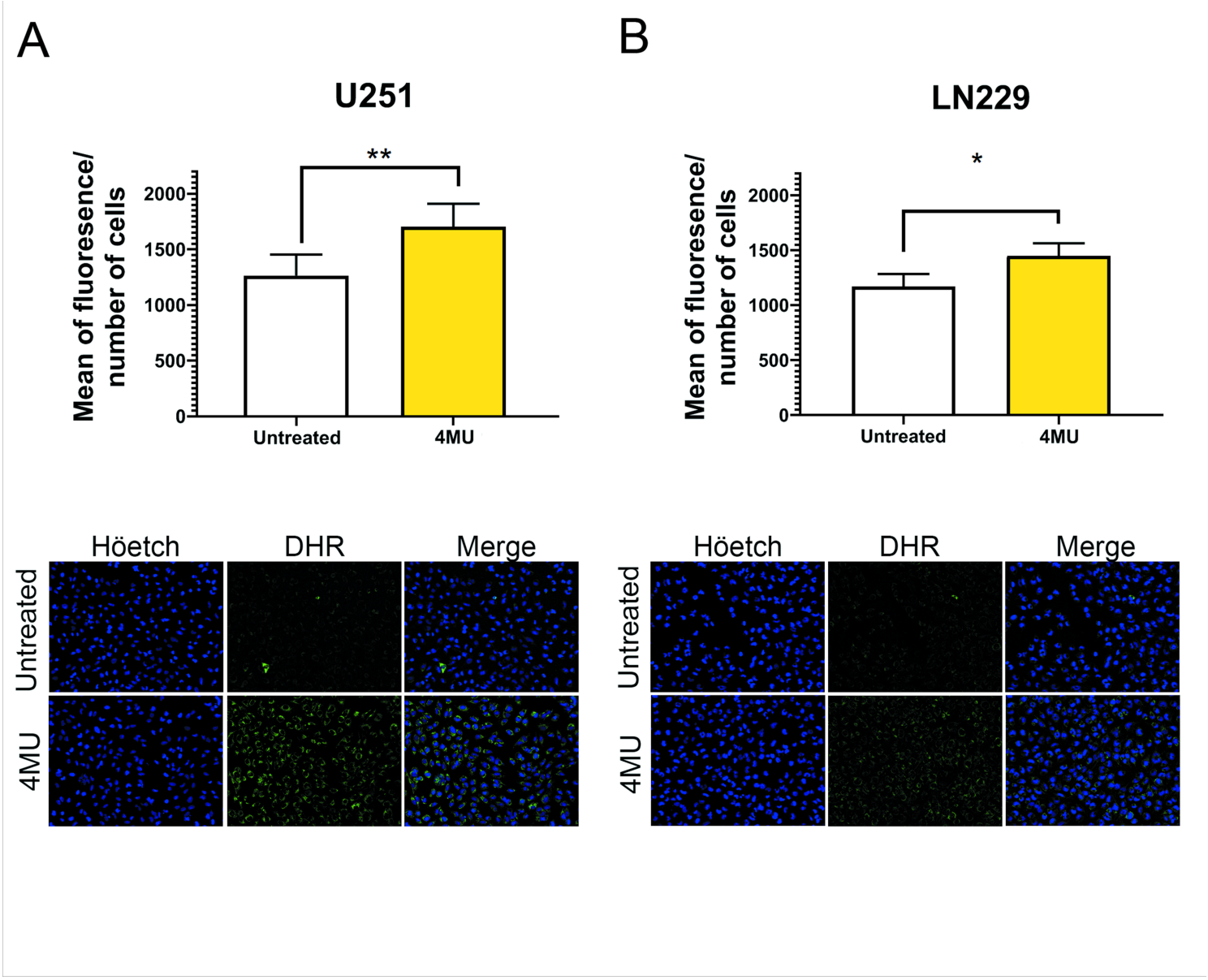


Figure 5

4MU effect on oxidative stress of GBM cells. (**A**) Cell redox state of U251 and LN229 cells was determined by DHR staining and microscopic observation, as described in Materials and Methods section. Results are expressed as mean fluorescence of DHR-positive cells over total number of cells under 1000 µM 4MU treatment vs untreated. In all graphs, each bar represents the mean ± SD of at least 3 independent experiments. Asterisks (*) indicate differences between treated cells and vehicle control cells. *P<0.05, **P<0.01, ***P < 0.001, ****P < 0.0001 and ns = nonsignificant (P > 0.05). (**B**) Representative microphotographs of U251 and LN229 cells treated with 4MU and untreated, stained with Höetch and DHR as described in Materials and Methods section.

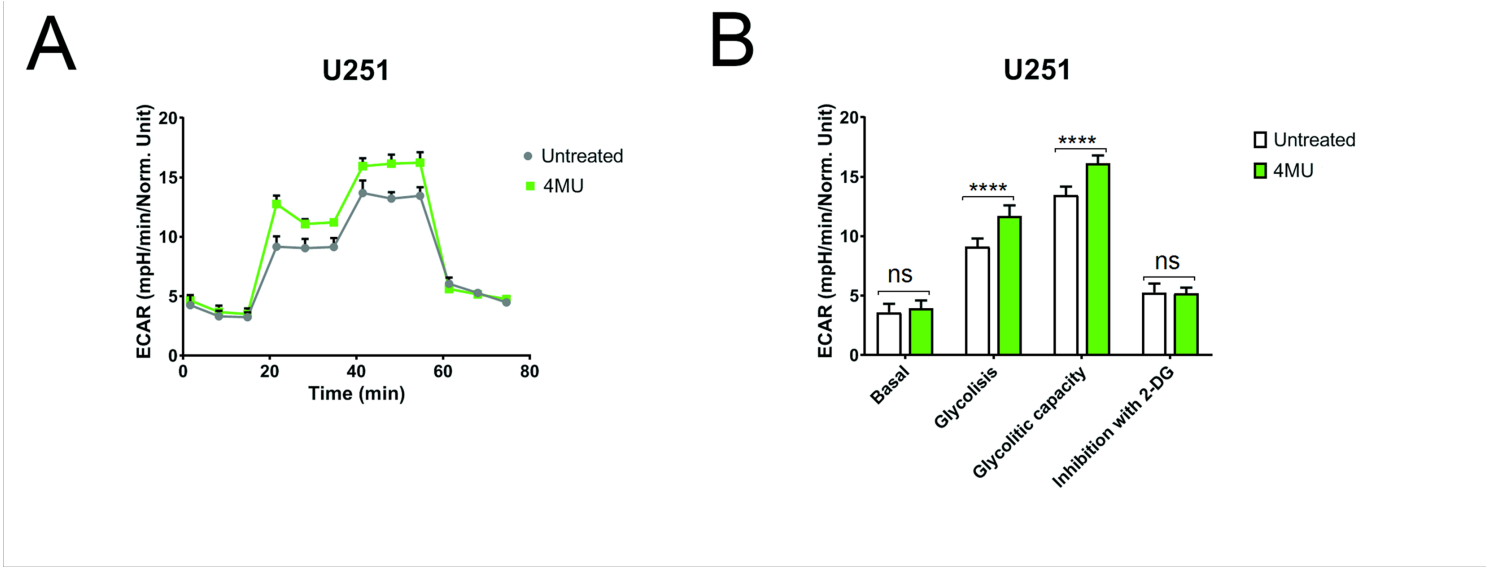


Figure 6

4MU effect on protein N-glycosylation of GBM cells. N-glycosylation of (**A**) U251 and (**B**) LN229 cells was determined by ConA and PHA-E binding analysed by flow cytometry, as described in Materials and Methods section. Results are expressed as mean fluorescence of cells under 1000 μM 4MU treatment vs untreated. In all graphs, each bar represents the mean ± SD of at least 3 independent experiments. Asterisks (*) indicate differences between treated cells and vehicle control cells. *P<0.05, **P<0.01, ***P < 0.001, ****P < 0.0001 and ns = nonsignificant (P > 0.05).

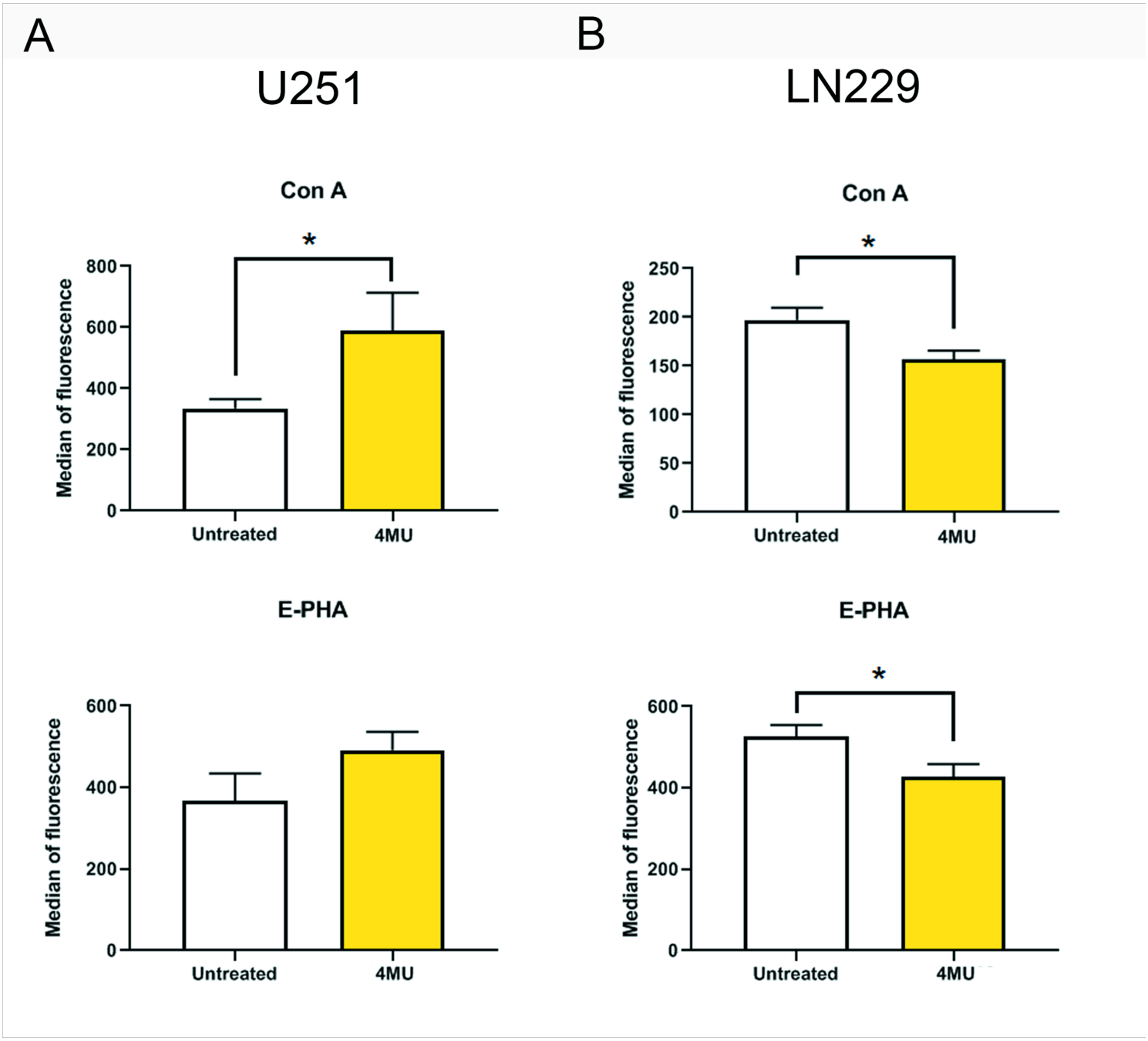


Figure 7

4MU effect on glycolytic flux of U251 cells. (**A**) Extracellular acidification rate (ECAR) profile through time, assessed after 24 h of treatment by Seahorse Glycolytic Stress Assay, as described in Materials and Methods section. (**B**) Comparison of each step of Glico-Stress Assay of 4MU-treated vs untreated U251 cells. In all graphs, each dot or bar represents the mean ± SD of at least 3 independent experiments. Asterisks (*) over each bar indicate differences between treated cells and vehicle control cells. *P<0.05, **P<0.01, ***P < 0.001, ****P < 0.0001 and ns = Non-significant (P > 0.05).